

Controlled transport of magnetic particles using soft magnetic patterns

Richard S. Conroy,^{1,2,a)} Gary Zabow,^{1,2} John Moreland,² and Alan P. Koretsky¹

¹Laboratory of Functional and Molecular Imaging, National Institute of Neurological Disorders and Stroke, National Institutes of Health, Bethesda, Maryland 20892, USA

²National Institute of Standards and Technology, 325 Broadway, Boulder, Colorado 80305, USA

(Received 27 June 2008; accepted 27 September 2008; published online 20 November 2008)

Inspired by magnetic bubble memory technology, we demonstrate the temporal and spatial manipulation of superparamagnetic beads guided by soft magnetic patterns in a rotating magnetic field. Soft magnetic structures allow complex and repetitive tasks to be performed. As a demonstration, we show cyclic capture and release of antibodies from different microfluidic streams. © 2008 American Institute of Physics. [DOI: 10.1063/1.3009197]

Magnetic particle manipulation is important in bio-science because of the need for separation and concentration of biomolecules and cells.¹ With the trend toward integrated microfluidic devices for micrototal analysis, micrometer-sized superparamagnetic beads provide convenient, scalable and inexpensive methods for trapping and transporting tagged biological entities.²

In addition to separation and concentration in static fluids, magnetophoresis has been used to bind and release unidirectionally from channels in a microfluidic system.³ However simultaneous temporal and spatial control of large ensembles of particles are difficult to achieve without microscopic patterning. Microfabricated core/coil designs⁴ and soft magnetic structures⁵ have been made for catch-and-release temporal separation of superparamagnetic particles. Additionally, microfabricated current carrying wires,⁶ meshes,⁷ and micropatterned conductors⁸ have been used for both trapping and transport of magnetic particles. However, current-driven systems are limited to small numbers of particles and low forces by heating and complexity concerns.

To address these issues, microstructured permanent magnetic surfaces have been used to manipulate a wide range of particles including cold atoms,⁹ leading to the idea of a “magnetic washboard”¹⁰ over which particles could be transported and split using a rotating magnetic field. Using this approach, the separation of a mixed population of microorganisms labeled with magnetic beads was demonstrated recently.¹¹

In this letter we describe a complementary approach to both current-carrying wires and permanent magnetic structures to trap, transport, and release magnetic particles. As realized by the designers of magnetic bubble memory,¹² soft magnetic structures can add flexibility by enabling the simultaneous motion of magnetic domains in arbitrary directions in a rotating external magnetic field. Thus bidirectional motion and closed loops could be designed in a memory chip that would not be possible with permanent magnetic structures and at a density and level of parallelism that would be much harder to achieve with current carrying wires. Here we build on this insight to show how soft magnetic structures can trap, transport, and release superparamagnetic particles with active control in position and time. Alternative means of

effecting transport with soft magnetic material have been demonstrated that depend on variations in partial magnetization saturation levels due to geometrical anisotropies of the materials.¹³ Here however, we present a more general approach that does not depend on partial saturation, but simply on translatable local field maxima created by variations in local radii of curvature at structural edges. In this way, analogs to the full repertoire of magnetic bubble memory manipulation schemes become available with the superparamagnetic beads shepherded around by the translatable local maxima that result from the summation of an external field and the local field from the magnetizable pattern.

Trapping and transport can be understood with a magnetic surface charge model,¹⁴ where the magnetic surface charge density, and hence the energy potential experienced by a superparamagnetic bead close to the surface, changes with the direction of the rotating field. In this model, charge concentrates at small radii of curvature parallel to the magnetic field, providing the deepest trapping potentials. Figure 1 illustrates some designs including [Fig. 1(a)] continuous and [Fig. 1(b)] discrete patterns from bubble memory technology, and [Fig. 1(c)] simultaneous bidirectional and [Fig. 1(d)] unidirectional movement of two beads. Qualitatively, unidirectional movement independent of the direction of rotation of the magnetic field, is characterized by shapes with a sharp point along the travel axis [Figs. 1(b) and 1(d)]. Movement which can be reversed with the direction of the magnetic field, is characterized by offset sharp points on either side of the shapes perpendicular to the travel direction [Figs. 1(a) and 1(c)]. Although our subsequent experiments focus on the saw-tooth design in Fig. 1(a) because of this reversible motion, many alternative magnetic bubble memory designs should be generally applicable in manipulating superparamagnetic particles.

The patterns illustrated in Fig. 1 were microfabricated through a photolithographically defined patterned etch through a 1 μm thick nickel layer that had been electrochemically deposited onto a 100 nm gold seed layer on top of a 10 nm titanium adhesive layer evaporated onto a glass substrate. Subsequently exposed sections of the gold seed layer were also selectively etched to enable optical access from both above and below the chip and a 7 μm thick layer of photoresist was spun over the shapes and hard baked.

The fabrication of the microfluidic channels used in these experiments has been described previously.¹⁵ Briefly, polydimethylsiloxane (PDMS) channels were patterned us-

^{a)}Author to whom correspondence should be addressed. FAX: 301-480-2558. Tel.: 301-435-4362. Electronic mail: conroyri@mail.nih.gov.

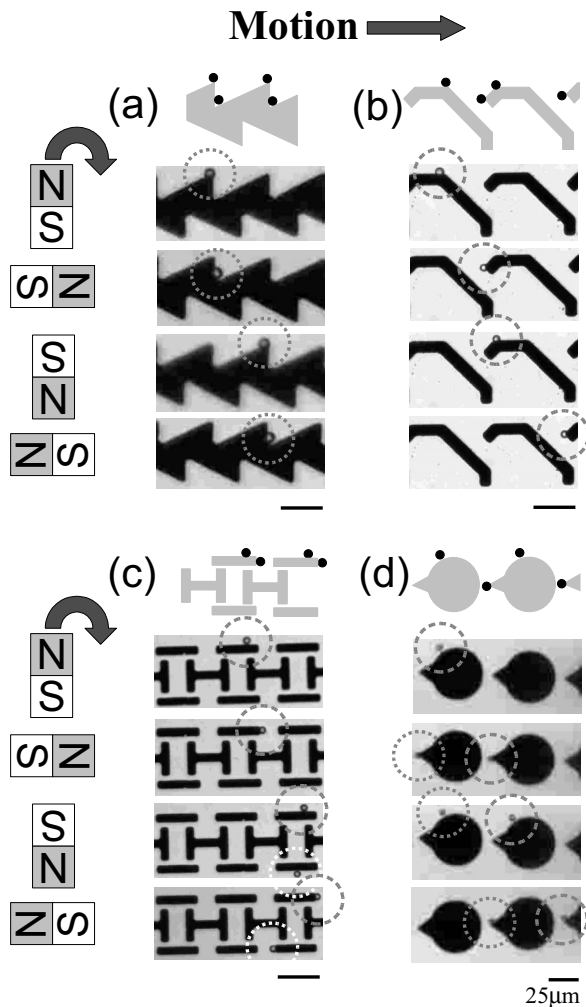


FIG. 1. A selection of periodic patterns that can trap and transport superparamagnetic particles by rotation of an external magnetic field. The vertical sequence of micrographs below each schematic representation of the pattern and particle movement shows the position of an $8\ \mu\text{m}$ diameter superparamagnetic particle (highlighted by gray circles) as the external field of $40\ \text{mT}$ is rotated 90° steps clockwise. (c) The micrographs illustrate the movement of two particles in antiparallel directions for the same field rotation, the top bead (gray) moving left to right and the lower bead (white) moving right to left on the opposite side of the pattern. (d) The micrographs illustrate two particles moving in the same direct in phase with each other.

ing an SU8 photoresist mold. Holes punched into the PDMS mask provided fluid inlets and this mask was then brought into conformal contact with the photoresist-covered magnetic structures to seal the channel. A schematic of the construction is shown in Fig. 2.

To create laminar flow in the microfluidic channel, three syringes mounted in programmable pumps were connected to the inlets. The external magnetic field was created using a cylindrical neodymium iron boron permanent magnet ($\phi = 25 \times 25\ \text{mm}^2$). The magnitude and orientation of the magnetic field was manipulated manually by varying the distance and orientation of the magnet. The microfluidic channel was imaged on an inverted microscope setup.

$8\ \mu\text{m}$ diameter superparamagnetic beads (Bangs Laboratories Inc., Fishers, IN) were suspended in phosphate buffered saline (PBS) (pH 7.4), supplemented with bovine serum albumin ($100\ \mu\text{g}/\text{ml}$) and Tween 20 (0.1%) to minimize nonspecific binding. For the antibody experiments in the microfluidic channel, anti-TREK-1 polyclonal antibodies

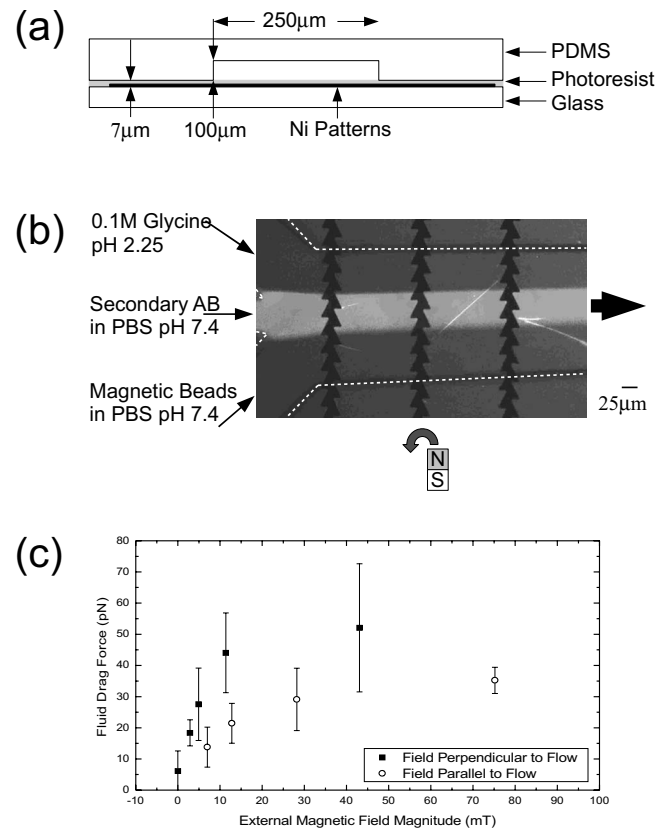


FIG. 2. Schematic and micrograph of the microfluidic setup. (a) Schematic representation of the cross section of the microfluidic channel. (b) Micrograph of a merged white light and fluorescence image to illustrate the laminar flow from the three inlets perpendicular to the saw-tooth pattern. The concentration of the secondary antibody was increased to $40\ \mu\text{g}/\text{ml}$ to collect this image. Dotted white lines have been added to emphasize the boundaries of the channel. (c) Average force and standard deviation from fluid drag in the microfluidic channel required to detach $8\ \mu\text{m}$ diameter superparamagnetic beads ($n=25$) from the setup in (b) depending on the orientation and magnitude of the external magnetic field.

from goat were covalently bound to the carboxyl groups on the surface of the beads with the zero-length cross-linker 1-ethyl-3-(3-dimethylaminopropyl)carbodi-imide (Pierce Biotechnology, Rockford, IL) using the manufacturer's suggested protocol. Complementary IgG antibodies labeled with Alexa Fluor 488 were used as a capture target. To dissociate the secondary antibody from the primary antibody, a 0.1M glycine buffer (pH 2.25) was used.

To test the transport properties of the shapes illustrated in Fig. 1, a $50\ \mu\text{l}$ drop of buffer containing 0.001% (w/v) beads was placed on the photoresist layer. Superparamagnetic beads between 1 and $10\ \mu\text{m}$ in diameter were tested. For external field strengths of more than $10\ \text{mT}$, all of the particles could be trapped and transported, with the largest beads transported most efficiently. For an external field of $40\ \text{mT}$, the capture radius for each shape was approximately its half width. By rotating the external magnetic field in the plane of the structures, the beads were translated smoothly along the edge of the patterns as illustrated in the lower micrographs of Fig. 1, with a velocity of up to $10\ \mu\text{m}/\text{s}$, limited by the manual rotation speed of the magnet.

To quantify the magnetic trapping force, the Stokes drag force was balanced against the attractive force of the magnetic field gradient.¹⁶ The microfluidic setup illustrated in Fig. 2 was used, with all three inlets containing $8\ \mu\text{m}$ beads

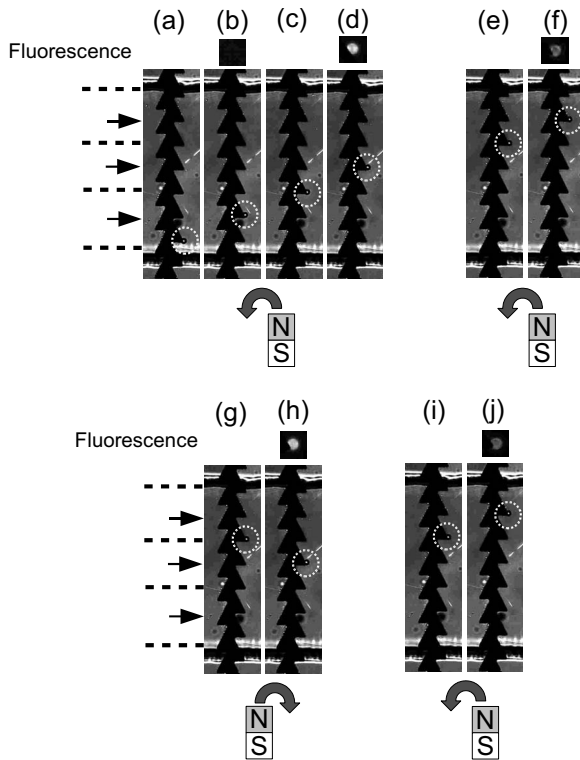


FIG. 3. Sequential brightfield micrographs illustrating the trapping and controlled transport of magnetic beads between streams in a microfluidic channel. (a) Superparamagnetic beads are captured from the lower stream in the micrographs and transported into the middle stream [(a)–(d)] where the bead is held for 5 min to accumulate complementary fluorescent secondary antibody, as illustrated in the enlarged fluorescent images of the bead. These antibodies can be dissociated from the bead by moving it into the upper stream [(e)–(f)] and holding it there for 5 min. This process can be repeated by first rotating the external field clockwise [(g)–(h)] to move the bead back into the middle stream, holding it for 5 min and then rotating the field anticlockwise [(i)–(j)] to move the bead back to the upper stream. The progress of the bead has been highlighted by a dotted white circle.

in the PBS buffer. After capturing beads at the maxima of the patterns using the external field, the flow rate was increased until the beads detached. The orientation of the magnetic field is important in determining the extent of the potential the magnetic particle experiences. For field directions perpendicular to the flow, the particle has a larger trapping volume in the flow direction bounded by the two sharp corners, while for field directions parallel to the flow the trapping volume is smaller and limited to the outer corner. The large standard deviation in the bead detachment force is attributed to residual nonspecific interactions and the variation in the magnetization of the beads.

To demonstrate the potential of this technique the same microfluidic configuration was used for the capture of functionalized magnetic beads, which were then used for the repeated capture and release of antibodies by translocating them between streams. Figure 2(b) illustrates the configuration used for this experiment. The nonfluorescent $8\ \mu\text{m}$ diameter magnetic beads, labeled with anti-TREK-1, enter the microfluidic channel at $1\ \mu\text{l}/\text{min}$ in the channel closest to the magnet. When a bead is captured, it can be translated away from the magnet and into the middle stream by rotating the magnet anticlockwise as illustrated in Fig. 3. The complementary fluorescent secondary antibodies, at a concentration of $1\ \mu\text{g}/\text{ml}$ in the middle stream, were then cap-

tured on the surface of the bead. After a 5 min stationary period, the bead was then moved into the third stream, containing 0.1M glycine at $\text{pH}\ 2.25$. Under these acidic conditions the secondary antibody was eluted resulting in a decrease in fluorescence to a residual background due to incomplete elution. By rotating the magnet in a clockwise direction to reverse the direction of motion, the bead was moved back into the second channel to collect more secondary antibody before being moved back into the third channel to release its second payload. Although this capture and release process is not 100% efficient, it illustrates the flexibility of manipulation.

In conclusion, the use of an external control field has advantages over current-carrying wires of no heat dissipation and no increase in complexity for massively parallel manipulation, because connectors and addressable wires are not required. In addition soft magnetic structures allow continuous synchronized movement of many beads in arbitrary directions, limited only by the maxima defined by the pattern used and the capture efficiency for discrete beads.

The trapping forces reported here are comparable to optical and magnetic tweezers.¹⁶ Reducing the thickness of the covering photoresist, making the shapes from a higher permeability alloy or iron, and increasing the external field strength would increase trapping forces and enable the topology of the shapes to be exploited as well. Alternatively embedded magnetic structures would remove the need to consider topology. In addition, external electromagnets could be used to automate the process of capture and transport and increase transport rates.

The diversity of operations implemented in magnetic bubble memory devices illustrates how this approach can be scaled and adapted, complementing existing methods for trapping and transport of magnetic particles.

¹N. Pamme, *Lab Chip* **6**, 24 (2006).

²A. Y. Fu, H. P. Chou, C. Spence, F. H. Arnold, and S. R. Quake, *Anal. Chem.* **74**, 2451 (2002).

³S. A. Peyman, A. Iles, and N. Pamme, *Chem. Commun. (Cambridge)* **10**, 1220 (2008).

⁴Q. Ramadan, V. Samper, D. Poenar, and C. Yu, *Biomed. Microdevices* **8**, 151 (2006).

⁵J. H. Koschwanez, R. H. Carlson, and D. R. Meldrum, *Rev. Sci. Instrum.* **78**, 044301 (2007).

⁶T. Deng, G. M. Whitesides, M. Radhakrishnan, G. Zabow, and M. Prentiss, *Appl. Phys. Lett.* **78**, 1775 (2001).

⁷H. Lee, A. M. Purdon, V. Chu, and R. M. Westervelt, *Nano Lett.* **4**, 995 (2004).

⁸R. Wirix-Speetjens and J. de Boeck, *IEEE Trans. Magn.* **40**, 1944 (2004).

⁹E. A. Hinds and I. G. Hughes, *J. Phys. D* **32**, R119 (1999).

¹⁰D. Leibfried, E. Knill, C. Ospelkaus, and D. J. Wineland, *Phys. Rev. A* **76**, 032324 (2007).

¹¹B. B. Yellen, R. M. Erb, H. S. Son, R. Hewlin, H. Shang, and G. U. Lee, *Lab Chip* **7**, 1681 (2007).

¹²A. H. Bobeck, P. I. Bonyhard, and J. E. Geusic, *Proc. IEEE* **63**, 1176 (1975).

¹³K. Gunnarsson, P. E. Roy, S. Felton, J. Pihl, P. Svedlindh, S. Berner, H. Lidbaum, and S. Oscarsson, *Adv. Mater. (Weinheim, Ger.)* **17**, 1730 (2005).

¹⁴R. P. Williams, *IEEE Trans. Magn.* **17**, 2423 (1981).

¹⁵D. B. Wolfe, R. S. Conroy, P. Garstecki, B. T. Mayers, M. A. Fischbach, K. E. Paul, M. Prentiss, and G. M. Whitesides, *Proc. Natl. Acad. Sci. U.S.A.* **101**, 12434 (2004).

¹⁶C. Danilowicz, Y. Kafri, R. S. Conroy, V. W. Coljee, J. Weeks, and M. Prentiss, *Phys. Rev. Lett.* **93**, 078101 (2004).